Nanoscale

PAPER

View Article Online
View Journal | View Issue

Wet chemical synthesis of intermetallic Pt_3Zn nanocrystals *via* weak reduction reaction together with UPD process and their excellent electrocatalytic performances†

Cite this: *Nanoscale*, 2014, **6**, 7019

Qiaoli Chen, Jiawei Zhang, Yanyan Jia, Zhiyuan Jiang,* Zhaoxiong Xie* and Lansun Zheng

Platinum based alloy nanocrystals are promising catalysts for a variety of important practical process. However, it remains a great challenge to synthesize platinum-based intermetallic compound nanocrystals with well-defined surface structures. In this communication, taking the synthesis of concave cubic intermetallic Pt_3Zn nanocrystals with {*hk*0} facets as an example, we proposed a new synthesis strategy for intermetallic compounds by reduction of noble metal precursors *via* a slow reduction process and reduction of transition metal ions *via* an underpotential deposition (UPD) process in wet chemical synthesis. The as-prepared intermetallic Pt_3Zn nanocrystals exhibited superior CO poisoning tolerance and high electro-catalytic activity in both methanol and formic acid oxidation reactions in comparison with solid solution Pt_3Zn nanocrystals and Pt/C.

Received 17th January 2014
Accepted 11th March 2014

DOI: 10.1039/c4nr00313f

www.rsc.org/nanoscale

Introduction

The noble metal platinum attracts enormous research attention because of its extensive applications in various fields, such as in highly efficient catalysis for fuel cells, petroleum cracking and automotive exhaust processing.[1–4] Considering the low reserve and high cost of Pt catalysts, tremendous efforts have been devoted to increasing the catalytic efficiency and decreasing Pt utilization.[5–8] An impressive route is to alloy Pt with a non-noble metal component (*e.g.* Cu, Zn, Co, Ni) to form Pt-based alloy nanocrystals (NCs), which not only reduce the overall Pt loading, with economic benefits, but also possess new physical and chemical properties due to synergistic effects.[9–12] Compared with solid solution alloys, the intermetallic compounds have long-range atomic order *via* arranging regularly two different types of atoms according to the stoichiometry. As a result, intermetallic compound NCs could display optimal physical and chemical properties such as highly efficient catalytic performance and excellent structural stability due to their favourable geometric and electronic effects.[12–17] For instance, ordered Pt_3Ti NCs obtained from annealing disordered Pt_3Ti NCs at 600 °C exhibited higher activities for both formic acid and methanol oxidation than solid solution Pt_3Ti NCs.[17] However, it is difficult to synthesize controllably intermetallic alloys compared to solid solution alloys, because of the need to achieve both alloy formation and the ordered structure during the crystal growth process.[18–21] Traditionally, intermetallic compound NCs could be obtained *via* annealing of solid solution alloys at high temperature as intermetallic compounds usually represent thermodynamically stable phases.[12–17] Unfortunately, these methods offer little control over morphology and surface structure of the NCs, which usually affect greatly the performance of the materials.[22–25] As a matter of fact, low temperature wet chemical synthesis could be one of the best ways to synthesize intermetallic compound NCs with a specific morphology or surface structure. For the wet chemical synthesis, strong reducing agents are usually applied to achieve the simultaneous reduction of precursors of alloy components due to the distinct standard reduction potential (SRP). However, in this case the ordered intermetallic structures are difficult to form, because the rapid reduction of both metal precursors usually leads to the formation of solid solution alloys. A relatively slow rate of reduction and crystal growth by employing weak reductants at relatively low temperature could facilitate the structural and morphological control of intermetallic alloy NCs. Herein, taking the synthesis of a Pt_3Zn intermetallic compound as a typical example, an underpotential deposition (UPD) based strategy was developed to synthesize intermetallic compound NCs with high-index facets. The UPD of Zn atoms greatly reduces the difference in SRP between Zn and Pt precursors, which aids the simultaneous reduction of Zn and Pt precursors in mild conditions. It is also demonstrated that the as-prepared concave cubic intermetallic Pt_3Zn NCs possess

State Key Laboratory of Physical Chemistry of Solid Surfaces, Department of Chemistry, College of Chemistry and Chemical Engineering, Xiamen University, Xiamen, 361005, P.R. China. E-mail: zyjiang@xmu.edu.cn; zxxie@xmu.edu.cn

† Electronic supplementary information (ESI) available: Additional characterization data. See DOI: 10.1039/c4nr00313f

excellent CO-tolerance capacity and exhibit high electrocatalytic activity towards the electro-oxidation of methanol as well as formic acid.

Experimental

Chemicals and materials

Platinum(II) acetylacetonate ($Pt(acac)_2$), zinc(II) acetylacetonate ($Zn(acac)_2$), *n*-octylamine (tech 99%) were purchased from Alfa Aesar; *N*,*N*-dimethylformamide (DMF), poly(vinylpyrrolidone) (PVP) (K-30, AR) were purchased from Sinopharm Chemical Reagent Co. Ltd. (Shanghai, China). All reagents were used as received without further purification.

Synthesis of concave cubic intermetallic Pt_3Zn NCs

In a 25 mL Teflon-lined stainless-steel autoclave, 16.8 mg $Pt(acac)_2$, 10.0 mg $Zn(acac)_2$ and 320.0 mg PVP were dissolved in 10.0 mL DMF. The sealed vessel was then heated to 180 °C and stayed for 9 h before it was cooled to room temperature. The black nanoparticles were collected by centrifugation, and further cleaned by ethanol.

Synthesis of solid solution Pt_3Zn alloy NCs

In a 25 mL Teflon-lined stainless-steel autoclave, 16.8 mg $Pt(acac)_2$, 10.0 mg $Zn(acac)_2$ and 320.0 mg PVP were dissolved in 10.0 mL DMF. In addition, 50 μL *n*-octylamine were added to the mixture. The sealed vessel was then heated to 180 °C and kept for 9 h before it was cooled to room temperature. The black nanoparticles were collected by centrifugation, and further cleaned by ethanol.

Characterization

Powder X-ray diffraction (XRD) patterns were recorded on a Rigaku Ultima IV diffractometer (Cu Kα, $\lambda = 1.54056$ Å) to study the crystallographic and compositional information of the samples. The morphology and crystal structure of the as-prepared products were observed by scanning electron microscopy (SEM, Hitachi S4800) equipped with energy dispersive X-ray spectroscopy, and transmission electron microscopy (JEOL JEM 2100). High-angle annular dark-field scanning transmission electron microscopy (HAADF-STEM) and energy-dispersive X-ray spectroscopy (EDS) were performed on a FEI TECNAI F30 microscope operated at 300 kV. All TEM samples were prepared by depositing a drop of diluted suspension in ethanol on a copper grid coated with carbon film.

Electrochemical measurements

Glassy carbon electrodes (diameter of 5 mm) were first carefully polished and washed before each experiment. Then, the ethanol suspensions of the as-prepared concave cubic intermetallic Pt_3Zn NCs were transferred to the surface of the glassy carbon electrode and dried at room temperature. The cyclic voltammetry (CV) measurements were performed on an electrochemical workstation (CHI 1030b, Shanghai Chenhua Co., China). A Pt sheet was employed as the counter electrode, and a saturated calomel electrode (SCE) was used as the reference electrode. All the electrode potentials here are quoted *versus* the SCE. Before measurement, the working electrode loaded with the as-prepared concave cubic intermetallic Pt_3Zn NCs was electrochemically cleaned by continuous potential cycling between −0.20 and 0.90 V at 50 mV s^{-1} in 0.10 M H_2SO_4 solution until a stable cyclic CV curve was obtained. The electrochemically active surface area (ECSA) of the catalysts was calculated by the equation ECSA = Q/q_0, in which Q is determined by the area of the hydrogen adsorption peaks in the cyclic voltammetry measurement performed in H_2SO_4 electrolyte (25 °C), and q_0 is 210 μC cm^{-2}. Methanol oxidation is tested in the solution of 0.10 M H_2SO_4 + 0.50 M methanol at a scan rate of 50 mV s^{-1}. The catalytic activity of concave cubic intermetallic Pt_3Zn NCs towards electro-oxidation of formic acid was measured in the solution of 0.50 M H_2SO_4 + 0.25 M formic acid at a scan rate of 50 mV s^{-1}. For the CO-stripping voltammetry measurements, CO gas (99.99%) was bubbled for 15 min through the H_2SO_4 solution (0.10 M) in which the electrode was immersed. Then the electrode was quickly moved to a fresh solution purged by N_2 and the CO-stripping voltammetry was recorded at a sweep rate of 20 mV s^{-1}. For the characterization of solid solution Pt_3Zn NCs and Pt/C, the above processes were followed.

Results and discussion

Scheme 1 illustrates the designed scheme for the synthesis of Pt_3Zn intermetallic compound NCs *via* the UPD based wet chemical method. Firstly, a UPD process is needed undoubtedly to prevent the metallic Pt and Zn from growing separately in the synthetic process due to their different SRPs. The SRP of Pt^{2+}/Pt is 1.18 V while the SRP of Zn^{2+}/Zn is −0.76 V. Therefore Pt^{2+} ions are usually reduced prior to Zn^{2+} ions when they coexist. Fortunately, the redox potential of the Zn/Pt (UPD) substrate

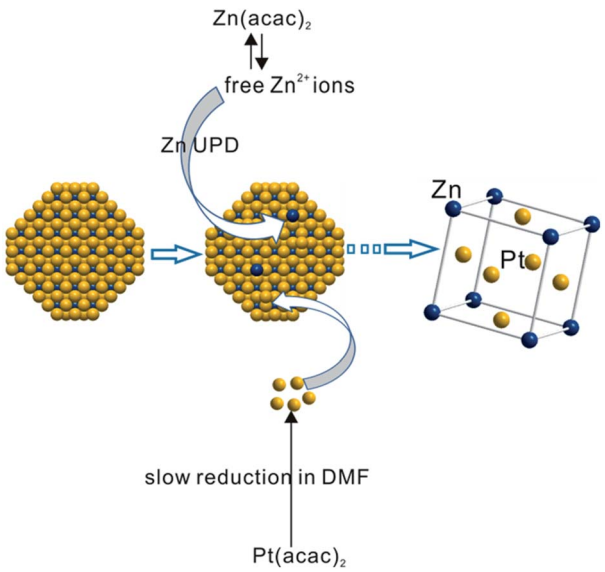

Scheme 1 Schematic diagram of a designed approach to the synthesis of Pt_3Zn intermetallic compound nanocrystals *via* a UPD based wet chemical method.

can be 1.44 V more positive than that of Zn^{2+}/Zn, and the calculated value is 0.58 V.[26] On the other hand, when platinum(II) acetylacetonate ($Pt(acac)_2$) was employed as a Pt precursor, the existence of acetylacetone ligands might help to keep a consistent supply of free Pt^{2+} *via* the complexation and lower the reduction potential.[27] Once the Pt^{2+} is reduced to Pt, the Zn^{2+} would be reduced subsequently through a quick UPD process. Note that the UPD is a sub-monoatomic layer deposition, which is blocked automatically when the whole surface is properly covered with sub-monoatomic layer of foreign metal atoms (*e.g.* Zn atom on Pt substrate). In this way, Pt^{2+} and Zn^{2+} could be reduced simultaneously at proper rates with a fixed composition, which results in the formation of Pt–Zn alloy NCs. Besides, to ensure the reduced Zn atom locates to an accurate position in the intermetallic compounds, mild reducing conditions were controlled by employing *N*,*N*-dimethylformamide (DMF) as a weak reducing agent.[9]

Fig. 1 shows the morphology and X-ray powder diffraction (XRD) pattern of the as-prepared products. The scanning electron microscope (SEM) image (Fig. 1a) of the product indicates the successful preparation of homogeneous NCs with a high yield. By carefully observation, it can be found that the NCs have a cube-like morphology with a side length of around 13 nm. The enlarged SEM image in the upper left of Fig. 1a shows the edge region is much brighter than the central region of the NCs, indicating the as-prepared NCs with concave features. The concave feature can also be deduced from the outline and the variation of image contrast of these cube-like nanoparticles in the typical transmission electron microscope (TEM) image of the as-prepared NCs (Fig. S1 in ESI†). It should be noted that the observed different outlines of the products are caused by the different orientations of the cube-like NCs. Besides the morphology, the structure and phase analysis of the as-prepared nanoparticles by XRD indicate the successful synthesis of intermetallic compound Pt_3Zn NCs as shown in Fig. 1b. All the diffraction peaks of the sample can be assigned to cubic intermetallic Pt_3Zn (JCPDS No. 65-3257). The cell constant *a* of the as-prepared NCs, which was refined to be 3.892(5) Å, also matches well with that of the standard intermetallic Pt_3Zn (3.893 Å). The composition detected by energy-dispersive X-ray spectroscopy (EDS) equipped on SEM (Fig. S2 in the ESI†), shows that the molar ratio of Zn in the alloy was about 24.9%, which is also close to the theoretical value of 25%. Furthermore, elemental mapping analysis (Fig. S3 in the ESI†) demonstrates that the distribution ranges of Pt and Zn are almost completely overlapped, supporting the successful preparation of intermetallic compound Pt_3Zn. To verify the surface structure of the concave Pt_3Zn nanocubes, an individual concave nanocube (Fig. 1c) was projected along the [001] axis, as confirmed by the corresponding SAED pattern and fast Fourier transform (FFT) pattern (inset of Fig. 1c). The continuous lattice fringes with a lattice spacing of 0.19 nm overspread the whole area of the NC in the HRTEM, indicating that the concave nanocube is a single crystal. The Miller indices of exposed facets of the concave nanocube can be identified by the angles between the exposed facets of the projected concave nanocube and the {100} facets of an ideal cube. The measured angles were 31°, 26° and 22°, as shown in Fig. 1c, which are consistent with the theoretical angle between the {530}, {210}, {520} and the {100} facets, respectively (see details in Table S1†). It can be concluded by measuring more concave nanocubes that the as-prepared NCs are mainly enclosed by {520} facets, together with some other high-index facets such as {530} and {210}. The schematic morphologic models of the concave nanocube with exposed {520} facets are therefore proposed and shown in Fig. 1d, which match well with the observed concave cubes along different directions. Based on the above results and discussion, it can be concluded unambiguously that the intermetallic Pt_3Zn alloy concave cubic NCs bound by high-index {520} facets had been successfully prepared *via* a UPD based method.

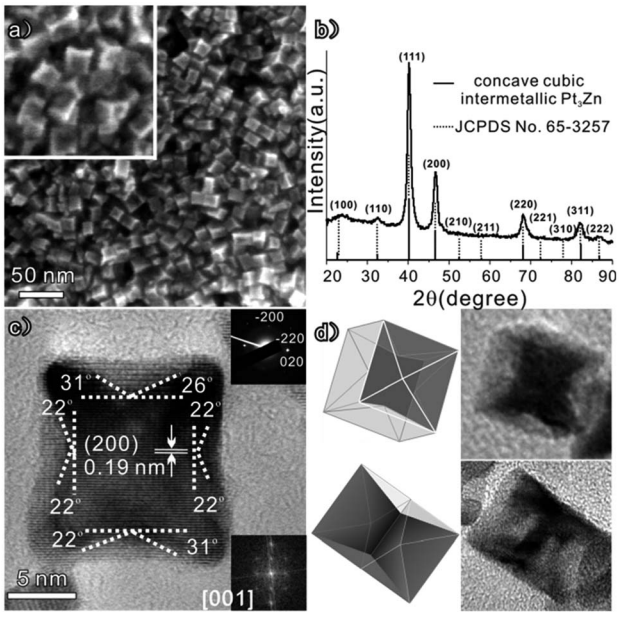

Fig. 1 (a) SEM image of the concave cubic intermetallic Pt_3Zn NCs on a large scale; the upper left inset of (a) is the enlarged SEM image. (b) XRD pattern of the concave cubic intermetallic Pt_3Zn NCs. (c) HRTEM image of an individual concave cubic intermetallic Pt_3Zn NC projected from the [001] direction, the upper and bottom right insets of (c) the corresponding SAED and FFT patterns of the concave cubic intermetallic Pt_3Zn NCs, respectively. (d) Schematic models of concave Pt_3Zn NC in different directions and the corresponding TEM images.

To confirm that the UPD process is necessary for the formation of intermetallic Pt_3Zn NCs, some experiments were designed and carried out. When taking $Pt(acac)_2$ as the only precursor in growth solution while keeping other conditions the same, pure Pt NCs of different sizes are produced (see the XRD pattern and SEM images in Fig. S4a and S4b†). In contrast, when $Zn(acac)_2$ was the only precursor, no Zn NCs can be found in the products after reaction in DMF for 24 hours. Instead, wurtzite ZnO NCs were formed due to thermal decomposition of $Zn(acac)_2$ (Fig. S4c†). Therefore, UPD of Zn^{2+} on a reduced Pt surface should be responsible for the formation of Pt–Zn alloy, as $Zn(acac)_2$ cannot be reduced solely. Further impressive evidence of the UPD process is the experimental results on controlling the reaction temperature. When the temperature

was decreased from 180 °C to 120 °C, at which the $Pt(acac)_2$ cannot be reduced to metallic Pt in DMF, no Pt–Zn alloys can be formed from the mixed solution of $Pt(acac)_2$ and $Zn(acac)_2$. Once the Pt ions could be reduced, such as when raising the temperature to 150 °C, intermetallic Pt_3Zn rather than pure Pt appeared. The reaction temperature was optimized to 180 °C as the reaction is too slow at 150 °C.

It should be pointed that the $Pt(acac)_2$ is necessary in the present case because it can not only keep a consistent supply of free Pt^{2+} for the slow reducing rate of Pt^{2+} to metallic Pt *via* the complexation of Pt^{2+} ions with acetylacetone ligands, but also lower the reduction potential.[27] By replacing $Pt(acac)_2$ with H_2PtCl_6 or K_2PtCl_4, all products are Pt NCs (see corresponding XRD patterns and TEM images in Fig. S5 in the ESI†), which could be due to a relatively positive reduction potential and fast reducing rate of H_2PtCl_6 or K_2PtCl_4 to metallic Pt. Accordingly, a proper reducing rate of Pt precursor ensures the formation of Pt–Zn alloy. In addition, it is found the surface status of Pt nuclei is also essential for Pt and Zn atoms to seek the most stable structure position to form the intermetallic Pt_3Zn alloy with long-range atomic order. Fig. 2 shows the XRD patterns of the products by adding different amounts of *n*-octylamine, which can bind to the surface of Pt strongly,[1,3] in the reaction systems. When the amount of the *n*-octylamine fed in the total 10 mL growth solution increased from 0 μL to 50 μL, the intensity of the (110) XRD peak (as marked by arrows in Fig. 2), which is the characteristic of the intermetallic Pt_3Zn phase, gradually decreased, and finally disappeared. The results indicate that the addition of *n*-octylamine would impede the movement of Pt and/or Zn atoms to seek an accurate position due to its strong adsorption with Pt nuclei, which results in growth of the Pt–Zn alloy NCs with a solid solution structure. For the effect of PVP, the contrast experiment showed that it is beneficial to homogeneity and dispersivity of the product (see Fig. S6 in ESI†).

Low-temperature fuel cells fed with small organic molecules have attracted extensive interest in the past decades. Pt-based NCs are the most active catalyst in these fuel cells. However, poor CO poisoning tolerance, a low reserve and the high cost of Pt severely limit their large-scale application. Therefore, it is urgent and important to improve the performance of Pt-based catalysts while reducing the consumption of Pt metal. Owing to their unique chemical composition and surface structure, the as-prepared concave cubic intermetallic Pt_3Zn NCs should have improved catalysis performance. It has been reported that the incorporation of exotic metal ions in Pt may modify the electronic structure of Pt and improve the ability of CO-poisoning tolerance towards electrocatalysis,[9,28] so the CO-tolerance properties of as-prepared concave cubic intermetallic Pt_3Zn NCs was firstly investigated *via* CO stripping, which is commonly used to probe the CO removal ability of the catalysts.[9,29] Commercial Pt/C and solid solution Pt_3Zn alloy NCs (see the ESI for the corresponding SEM image and TEM image in Fig. S7†) were used as the reference catalysts. As shown in Fig. 3a, the onset of CO stripping on concave cubic intermetallic Pt_3Zn NCs is lower than that on solid solution Pt_3Zn NCs and Pt/C by 71 mV, 192 mV, respectively (detailed in the ESI, Table S2†), and the main oxidation peak is also shifted negatively by about 42 mV and 79 mV, respectively. The above experiment demonstrates that Pt_3Zn intermetallic alloy NCs have the best CO removal ability, which might arise mainly from the optimum geometric, d-electron density and electronic structure of Pt modified by Zn.[13,14]

The excellent CO removal ability would greatly improve CO-tolerance towards the oxidation of some small molecules in the fuel cells. Therefore, methanol was chosen firstly as a benchmark to study the electrocatalytic activity of the as-prepared concave cubic intermetallic Pt_3Zn NCs. Fig. 3b shows CVs of methanol oxidation on concave cubic intermetallic Pt_3Zn NCs, solid solution Pt_3Zn NCs and Pt/C in a solution of 0.10 M H_2SO_4 + 0.50 M methanol at a scan rate of 50 mV s^{-1} (the corresponding CV in 0.10 M H_2SO_4 is shown in Fig. S8†). It has been well established that the electrochemical oxidation of methanol on Pt-based alloy proceeds preferentially through the indirect pathway, where methanol firstly undergoes dissociative

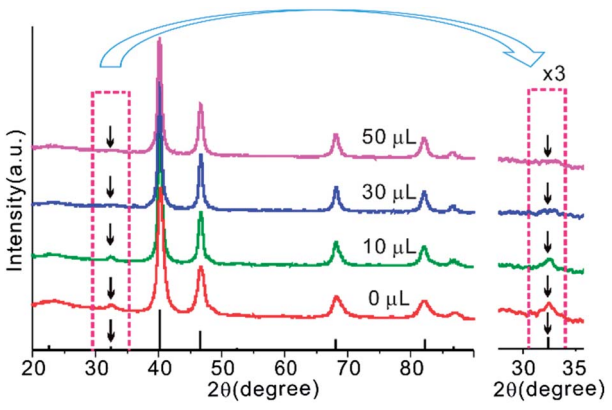

Fig. 2 XRD patterns of products obtained from different volumes of *n*-octylamine. The inset in the right part shows an enlarged view of (110) diffraction peaks.

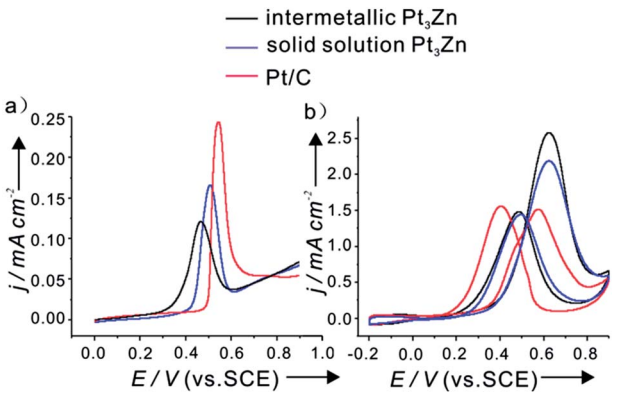

Fig. 3 CV curves measured on the concave cubic intermetallic Pt_3Zn NCs, solid solution Pt_3Zn NCs and commercial Pt/C: (a) CO-stripping curves in 0.10 M H_2SO_4 solution (scan rate: 20 mV s^{-1}). (b) Methanol oxidation in an 0.10 M H_2SO_4 + 0.50 M methanol solution (scan rate: 50 mV s^{-1}). All currents in electrochemical measurements were normalized to the corresponding electrochemical active surface area.

adsorption and electrochemical dehydrogenation to form CO_{ad}, then the CO_{ad} is oxidized. The latter is considered to be the rate-limiting step.[30,31] As shown in Fig. 3b, in the forward sweep, the peak at 0.62 V can be due to the formation of CO, CO_2 and other carbonaceous intermediates that adsorb onto the catalyst surface. During the backward sweep, an oxidation peak appears at 0.45 V, corresponding to the complete desorption of oxygen from the catalyst surface and further oxidization of carbonaceous species to CO_2. Usually, the ratio of the peak current densities between the forward (j_f) and backward scan (j_b) reflects the tolerance of the catalysts to the carbonaceous intermediate, and a higher j_f/j_b value usually indicates a better CO-tolerance.[9,32] For the concave cubic intermetallic Pt_3Zn NCs, solid solution Pt_3Zn NCs and commercial Pt/C, the peak current densities of the forward scan were 2.58, 2.19 and 1.51 mA cm^{-2}, respectively; and the corresponding backward peak current densities were 1.48, 1.44 and 1.56 mA cm^{-2}, respectively (Table S3 in the ESI†). The j_f/j_b ratio of the as-prepared concave cubic intermetallic Pt_3Zn NCs was 1.74 for methanol oxidation, while the ratio of solid solution Pt_3Zn NCs and commercial Pt/C was 1.52 and 0.97, respectively (Table S3 in the ESI†). Obviously, the experimental result was congruent with the above-mentioned analysis that the addition of Zn in Pt greatly improves the CO-tolerance. Furthermore, it can be clearly seen that, by incorporating Zn into Pt, the two types of Pt_3Zn possessed enhanced catalytic activities compared to the commercial Pt/C. The origin of the enhancement methanol oxidation should be attributed largely to the modified electronic structure of Pt. Besides, the as-prepared concave cubic intermetallic Pt_3Zn NCs exhibited higher catalytic activity than the solid solution Pt_3Zn alloy NCs, which could be attributed to the optimum geometric electronic structure and high-index facets of the intermetallic concave cubic Pt_3Zn NCs. Using formic acid (another common fuel molecule) as probe, the similar results, namely the excellent electrocatalytic activity arising from outstanding CO removal capacity can also be obtained (see Fig. S9 and the corresponding description in the ESI†).

Conclusions

In summary, a UPD based route was developed to synthesize intermetallic compound Pt-based alloy NCs. Zn UPD helps to decrease the difference between the SRPs of Pt^{2+} and Zn^{2+}, and makes it possible to simultaneously reduce Pt and Zn precursors at proper rates, resulting in the formation of alloy structures. The low reduction rate caused by weak reductant plays an essential role in the formation of the intermetallic compound structures. In addition, it is demonstrated that the as-prepared concave cubic intermetallic Pt_3Zn NCs possess excellent CO-tolerance capacity and exhibit high electrocatalytic activity towards the electrooxidation of methanol as well as formic acid, suggesting that the intermetallic Pt_3Zn NCs may be a promising catalyst for low-temperature fuel cells fed with small organic molecules. The UPD of metal ions on a foreign metal substrate is a common electrochemical phenomenon that has been studied extensively. It is reasonable to believe that the present strategy can be extended to synthesize other important intermetallic compound NCs.

Acknowledgements

This work was supported by the National Basic Research Program of China (Grant nos 2011CBA00508 and 2013CB933901) and the National Natural Science Foundation of China (Grant nos 21131005, 21333008, 21171141 and J1030415).

Notes and references

1 X. Q. Huang, Z. P. Zhao, J. M. Fan, Y. M. Tan and N. F. Zheng, *J. Am. Chem. Soc.*, 2011, **133**, 4718.
2 N. Tian, Z. Y. Zhou, S. G. Sun, Y. Ding and Z. L. Wang, *Science*, 2007, **316**, 732.
3 L. Zhang, D. Q. Chen, Z. Y. Jiang, J. W. Zhang, S. F. Xie, Q. Kuang, Z. X. Xie and L. S. Zheng, *Nano Res.*, 2012, **5**, 181.
4 T. Yu, D. Y. Kim, H. Zhang and Y. Xia, *Angew. Chem., Int. Ed.*, 2011, **50**, 2773.
5 Z. M. Peng and H. Yang, *Nano Today*, 2009, **4**, 143.
6 Y. H. Bing, H. S. Liu, L. Zhang, D. Ghosh and J. J. Zhang, *Chem. Soc. Rev.*, 2010, **39**, 2184.
7 H. Zhang, M. Jin and Y. Xia, *Chem. Soc. Rev.*, 2012, **41**, 8035.
8 A. Chen and P. Holt-Hindle, *Chem. Rev.*, 2010, **110**, 3767.
9 Y. Q. Jiang, Y. Y. Jia, J. W. Zhang, L. Zhang, H. Huang, Z. X. Xie and L. S. Zheng, *Chem. – Eur. J.*, 2013, **19**, 3119.
10 H. Yang, J. Zhang, K. Sun, S. Zou and J. Fang, *Angew. Chem., Int. Ed.*, 2010, **49**, 6848.
11 V. R. Stamenkovic, B. Fowler, B. S. Mun, G. Wang, P. N. Ross, C. A. Lucas and N. M. Markovic, *Science*, 2007, **315**, 493.
12 Y. J. Kang, J. B. Pyo, X. C. Ye, T. R. Gordon and C. B. Murray, *ACS Nano*, 2012, **6**, 5642.
13 L. F. Xiong and A. Manthiram, *J. Mater. Chem.*, 2004, **14**, 1454.
14 L. F. Xiong and A. Manthiram, *J. Electrochem. Soc.*, 2005, **152**, A697.
15 D. L. Wang, H. L. Xin, R. Hovden, H. S. Wang, Y. C. Yu, D. A. Muller, F. J. DiSalvo and H. D. Abruña, *Nat. Mater.*, 2012, **12**, 81.
16 S. Sun, C. B. Murray, D. Weller, L. Folks and A. Moser, *Science*, 2000, **287**, 1989.
17 H. Abe, F. Matsumoto, L. R. Alden, S. C. Warren, H. D. Abruña and F. J. DiSalvo, *J. Am. Chem. Soc.*, 2008, **130**, 5452.
18 A. K. Sra and R. E. Schaak, *J. Am. Chem. Soc.*, 2004, **126**, 6667.
19 B. M. Leonard, N. S. P. Bhuvanesh and R. E. Schaak, *J. Am. Chem. Soc.*, 2005, **127**, 7326.
20 N. H. Chou and R. E. Schaak, *J. Am. Chem. Soc.*, 2007, **129**, 7339.
21 W. Chen, R. Yu, L. L. Li, A. N. Wang, Q. Peng and Y. D. Li, *Angew. Chem., Int. Ed.*, 2010, **49**, 2917.
22 Z. Y. Jiang, Q. Kuang, Z. X. Xie and L. S. Zheng, *Adv. Funct. Mater.*, 2010, **20**, 3634.
23 L. Zhang, J. W. Zhang, Q. Kuang, S. F. Xie, Z. Y. Jiang, Z. X. Xie and L. S. Zheng, *J. Am. Chem. Soc.*, 2011, **133**, 17114.
24 J. W. Zhang, C. P. Hou, H. Huang, L. Zhang, Z. Y. Jiang, G. X. Chen, Y. Y. Jia, Q. Kuang, Z. X. Xie and L. S. Zheng, *Small*, 2013, **9**, 538.

25 A. X. Yin, X. Q. Min, W. Zhu, W. C. Liu, Y. W. Zhang and C. H. Yan, *Chem. – Eur. J.*, 2012, **18**, 777.
26 S. Taguchi and A. Aramata, *J. Electrochem. Soc.*, 1995, **396**, 131.
27 G. Durieux, M. Gerdin, C. Moberg and A. Jutand, *Eur. J. Inorg. Chem.*, 2008, 4236.
28 D. Y. Wang, H. L. Chou, Y. C. Lin, F. J. Lai, C. H. Chen, J. F. Lee, B. J. Hwang and C. C. Chen, *J. Am. Chem. Soc.*, 2012, **134**, 10011.
29 D. F. van der Vliet, C. Wang, D. Li, A. P. Paulikas, J. Greeley, R. B. Rankin, D. Strmcnik, D. Tripkovic, N. M. Markovic and V. R. Stamenkovic, *Angew. Chem., Int. Ed.*, 2012, **51**, 3139.
30 T. Iwasita, *Electrochim. Acta*, 2002, **47**, 3663.
31 E. Antolini, J. R. C. Salgado and E. R. Gonzalez, *Appl. Catal., B*, 2006, **63**, 137.
32 Z. Q. Niu, D. S. Wang, R. Yu, Q. Peng and Y. D. Li, *Chem. Sci.*, 2012, **3**, 1925.